

DOI of publisher version (Journal of Theoretical Biology, Elsevier, 537 (2022) 111023):

<https://doi.org/10.1016/j.jtbi.2022.111023>

# A 3D MATHEMATICAL MODEL OF COUPLED STEM CELL-NUTRIENT DYNAMICS IN MYOCARDIAL REGENERATION THERAPY

D. Andreucci<sup>1</sup>, A.M. Bersani<sup>2</sup>, E. Bersani, F.J. León Trujillo<sup>3</sup>, S. Marconi<sup>1</sup>

<sup>1</sup> *Department of Basic and Applied Sciences for Engineering, Sapienza University of Rome, Italy*

<sup>2</sup> *Department of Mechanical and Aerospace Engineering, Sapienza University of Rome, Italy*

<sup>3</sup> *Faculty of Engineering and Architecture, University of Lima, Peru*

## Abstract

Stem cell therapy is a promising treatment for the regeneration of myocardial tissue injured by an ischemic event. Mathematical modeling of myocardial regeneration via stem cell therapy is a challenging task, since the mechanisms underlying the processes involved in the treatment are not yet fully understood. Many aspects must be accounted for, such as the spread of stem cells and nutrients, chemoattraction, cell proliferation, stages of cell maturation, differentiation, angiogenesis, stochastic effects, just to name a few. In this paper we propose a 3D mathematical model with a free boundary that aims to provide a qualitative description of some main aspects of the stem cell regenerative therapy in a simplified scenario. The paper mainly focuses on the description of the shrinking of the necrotic core during treatment. The stem cell and nutrients dynamics are described through coupled reaction-diffusion problems. Proliferation, chemoattraction, tissue regeneration and nutrient consumption are included in the model.

**Keywords:** Convection-diffusion-reaction equations, Free boundary problem, Stem cell therapy, Myocardial regeneration.

# 1 Introduction

Stem cell-based therapy for the treatment of myocardial infarction and heart failure has received great attention in the last decades for its potential to reduce infarct size and improve cardiac function [1, 2]. Many types of stem cell populations have been considered for their self-renewing and multi-lineage differentiation capabilities [3–5]. Both preclinical and clinical studies seem to confirm the beneficial effects in many cases, even if the effectiveness of the treatment is still controversial [6–8]. The mechanisms that induce the observed improvements have also been debated. The evidence seems to suggest that the stem cells produce both direct effects, due to transdifferentiation into cardiac and vascular lineages, and indirect effects, due to the secretion of growth factors and molecules that induce paracrine actions [9]. As a result, the presence of the stem cells in the damaged tissue can activate the endogenous stem cells, inhibit apoptosis, induce angiogenesis, enhance cardiomyocyte proliferation, prevent ventricular remodeling, modulate immune and inflammatory response [10–12]. Nevertheless, the success of the therapy can depend on several factors, such as the type of cell population used for the therapy, the pre-treatment of the stem cells before implantation [13], the protocol of stem cell delivery in the injured tissue [14–16], the cell dose and the number and timing of administration. These factors can affect the stem cell survival, motility, proliferation and long-term engraftment [17, 18].

In such a complex scenario, a comprehensive mathematical model of the stem cell therapy for the myocardial regeneration is still far from being achieved. Many works can be found in the literature that assess some key aspects of the therapy and attempt to describe and quantify selected behaviors of the stem cells, some of which based and tuned to *in vitro* experiments (see, for example, [19] for a nice review). Mathematical models describing stem cell peculiarities can be found not only in myocardial regeneration related works, but also in studies related to the employment of stem cells in the treatment of tumors or wound healing [20]. The main described aspects are: proliferation, self-renewal and differentiation [21–31]; motility and migration [32–35]; cell behavior on artificial scaffolds [36–38]; chemotaxis [39–42].

In this paper we are mainly interested in the description of the evolution of the geometry of the regenerated tissue and, consequently, of the shrinking of the necrotic core. Diffusion-reaction equations are widely used to describe a great variety of chemical and biological processes [43–47]. In this paper we aim to investigate the possibility of employing a free boundary problem for a

convective-diffusion-reaction equation to describe the stem cell dynamics in a regeneration therapy framework [48,49]. We consider the phase of the therapy where the stem cells have been already delivered to the heart with a single administration, for example via injection, or by means of different protocols, as those ones described in [14–16], and start permeating the inflamed region around a necrotic portion of the cardiac tissue. The regeneration of the tissue is achieved due to the arrival of the stem cells attracted by chemotaxis around the necrotic tissue. The structure of the partial differential equation stated in the model allows to describe cells migration, proliferation and death. The free boundary conditions allow to describe the shrinking of the boundary of the necrotic core during treatment.

We also consider another aspect of the therapy strictly linked to the presence of stem cells in the tissue, that is the diffusion and consumption of nutrients [50–54]. To this aim, we couple the differential problem describing the stem cell dynamics with an initial-boundary value problem for a diffusion-reaction equation describing the dynamics of nutrients in the considered domain. We analyse how the coupling between the two differential problems enables to describe the two concomitant processes and their mutual interactions.

The model is a three-dimensional one on a simple geometry. Moreover, as a first step toward the understanding of these processes, we simplify the model, making some arbitrary assumptions on the amount of cells that enter the inflamed region, the migration of the cells in the tissue, the way the stem cells are attracted toward the necrotic tissue, the proliferation rate, the deformation of the necrotic core and the consumption of the nutrients. Our purpose here is to analyse how the differential problems that we have established can capture some characteristic features of the stem cell therapy and verify how the simulations can help to interpret the behaviors described by the model.

The remainder of the paper is organized as follows: Section 2 describes the proposed model; Section 3 explains the methods used to implement the model; in Section 4 the simulation results in two different cases are presented; Section 5 is devoted to the discussion of the results and conclusions.

## 2 Model description

The main features of the proposed model are the diffusion and convection of stem cells through the inflamed region and the growth of the regenerated region into the necrotic core, or regeneration. Other important effects would be incorporated in the model in a future work, but we believe that the aforementioned features are essential to the very idea of a spatially distributed, diffusion based model of myocardial regeneration through stem cells.

The domain of the diffusion phenomenon is a small portion of the inflamed cardiac tissue and is represented by a subset  $D(t)$  of an ellipsoid  $E$ , to be deformed by regeneration. The complement of  $D(t)$  in  $E$  is the necrotic core  $N(t)$ ; at the initial time  $t = 0$ ,  $N(0)$  is a smaller concentric ellipsoid inside  $E$ . In the prototypical problem considered here the stem cells are implanted in a portion  $A$  of the external boundary of  $D$ , which is also the boundary  $\partial E$  of  $E$  (Figure 1); the concentration of the implanted cells is assumed to vanish with a prescribed law.

As already pointed out in the Introduction, we consider the phase of the therapy where the stem cells have been already delivered to the heart with a single administration, by means of a suitable protocol (injection, implantation etc.) and enter the inflamed region  $D$ . Obviously, the way the stem cells enter  $D$  could change depending on the protocol, but in this preliminary model we suppose that the cells, starting from the same part of the boundary  $\partial E$ , i.e.,  $A$ , move toward the necrotic core, passing through the inflamed zone. Of course other delivery protocols can be considered by adjusting the boundary conditions.

Due to diffusion and convection caused by chemoattraction, the stem cells migrate toward the necrotic area and arrive on its external surface  $\Gamma(t)$ . In this compartment of the model, the coupling of the transport equation for stem cells with the one for nutrients is of course of great importance. Here we lump all the nutrients in one species  $n$ , though in a more realistic scheme one would need more (oxygen, glucose, ...).

The presence of stem cells on the boundary of the necrotic core promotes the regeneration of heart tissue. As a result, the necrotic zone contracts and its boundary  $\Gamma(t)$  moves inward. In fact the process of deposition and differentiation of the stem cells is far from being trivial (see, for example, [55, 56]); however, we think that in a model taking into account the geometry of growth of regenerated tissue into the necrotic one, we necessarily must have a device explicitly linking the differentiation of stem cells to the volume gain

against the necrotic core. In our present scheme, we neglect in practice all differentiation steps, and assume that deposition and differentiation coincide (a possible fraction of unsuccessful differentiation is accounted for by the choice of the parameter  $\lambda$ , see below). By the same token, we assume that all stem cells arriving at  $\Gamma(t)$  are removed from diffusion by deposition. In this way we preserve the basic interplay between the stem cell concentration and the regeneration process. In a future model, this module will be expanded, leading to the coupling of the law for the growth rate of  $\Gamma(t)$  with the local cascade of differentiation.

Since in this paper we are mainly interested in the description of the first phase, consisting in the evolution of the geometry of the regenerated tissue, we don't yet consider the successive phase, when the stem cells differentiate. The simplification proposed above leads us to gather all stem cells in a single cell population, without distinguishing between the different stages of cell maturation [27, 28].

The unknowns of the model are the stem cell concentration  $s$  and the nutrients concentration  $n$  within the domain. They are functions of space and time (refer to Table 1 for a list of the symbols). The stem cell dynamics is described by a free boundary problem that accounts for cell diffusion, chemoattraction, proliferation, death and tissue regeneration. In parallel, nutrients dynamics is described with an initial-boundary value problem for a diffusion-reaction equation, coupled to the previous one, that accounts for nutrients diffusion and consumption. A condition on the nutrient flow from outside can also simulate the effect of angiogenesis in the considered domain.

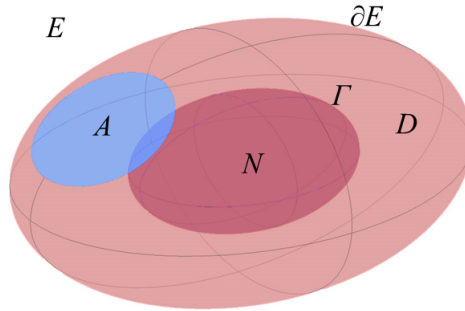


Figure 1: Schematic 3D representation of the inflamed and necrotic portion of cardiac tissue.  $D$ : inflamed region;  $N$ : necrotic core;  $E = D \cup N$ .  $N$  and  $E$  are supposed ellipsoidal.  $\partial E$ : external boundary of  $D$ ;  $\Gamma$ : external boundary of  $N$ , interface between  $N$  and  $D$ ;  $\partial D = \partial E \cup \Gamma$ ;  $A$ : stem cell implantation zone on the external boundary of  $D$ .

Symbol	Description
$E$	Portion of cardiac tissue
$D$	Inflamed region
$N$	Necrotic core
$\partial E$	External boundary of $D$
$A$	Stem cell implantation site on $\partial E$
$\Gamma$	Interface between $D$ and $N$
$s$	Stem cell concentration
$n$	Nutrient concentration

Table 1: List of the symbols; here all objects depend on time, excepting  $\partial E$  and  $A$ .

## 2.1 Stem cells dynamics

Here and in the sequel we omit to denote the dependence of the variables on the position  $\vec{x}$  and time  $t$ . The center of the ellipsoids is assumed to be the origin of the spatial coordinates. The dynamics of stem cells in  $D$  over the time interval  $[0, T]$  is governed by the diffusion-convection-reaction equation

$$\frac{\partial s}{\partial t} - \operatorname{div} \left( D_s \vec{\nabla} s - s \chi \hat{x} \right) = \mu_{max} \frac{n(1+K)}{n_{max}K+n} s \left( 1 - \frac{s}{s_{max}} \right) - R_d s. \quad (1)$$

The diffusion term describes cell motility. The diffusion coefficient  $D_s$  is an index of the ability of the cells to move in the surrounding tissue. The convective term  $s \chi \hat{x}$  describes the chemotaxis, that is the motion of the cells in response to chemical signals. Chemotaxis is commonly modeled with a convective term depending on a chemical gradient. We do not include the dynamics of the attractive chemical substances in this model and choose a radial attraction term instead. In principle, chemoattraction could depend on the distance from the necrotic core, but we simplify this condition and consider a constant attraction. The parameter  $\chi$  represents the sensitivity of the stem cells to the inward attraction. It is set up so that the chemotaxis dominates over diffusion.  $\hat{x}$  denotes the unit vector.

The reaction term has two contributions. The first one describes cell proliferation depending on the nutrients concentration  $n$ . The term in brackets prevents the stem cell concentration from growing beyond the maximum possible cell concentration in the tissue  $s_{max}$ : if  $s$  reaches the maximum value, the term in brackets becomes zero and proliferation stops. The remaining factors

can be written as  $\mu(n)s$  where  $\mu(n)$  is the proliferation rate. A Monod (or Michaelis-Menten) function, which classically describes saturation phenomena, is considered to define it:  $\mu_{max}$  and  $n_{max}$  are the maximum proliferation rate and the maximum nutrients concentration, respectively, while  $K$  is the half-saturation constant [50, 52, 57]. Finally, the second reaction term describes the cell death. The parameter  $R_d$  is the death rate.

In order to solve Equation (1), a set of initial and boundary conditions is imposed.

A null initial condition is set on the domain  $D(0)$ , as there are no stem cells inside  $D$  at the beginning of the process:

$$s(\vec{x}, 0) = 0 \quad \text{on} \quad D(0). \quad (2)$$

On the implantation site  $A$  we define a time dependent boundary condition  $BC(t)$  that describes the way the stem cells are implanted on the external boundary:

$$s(\vec{x}, t) = BC(t) \quad \text{on} \quad A. \quad (3)$$

We define the function  $BC$  as a smoothed decreasing step function from an initial concentration  $s_0$  to 0. The initial stem cell concentration on  $A$  gradually disappears in a limited initial interval of time.

We consider a Neumann condition on the rest of the external boundary:

$$D_s \frac{\partial s}{\partial \hat{\nu}}(\vec{x}, t) = 0 \quad \text{on} \quad \partial E \setminus A \quad (4)$$

where  $\hat{\nu}$  is the outer normal unit vector.

Finally, a null boundary condition is set on  $\Gamma$ :

$$s(\vec{x}, t) = 0 \quad \text{on} \quad \Gamma(t). \quad (5)$$

According to this condition, stem cells are absorbed by deposition on  $\Gamma$  and thus they do not reach the necrotic core, whose surface is made up of non-necrotic cardiac tissue. However, their presence induces the tissue regeneration and the consequent movement of the boundary. The inward normal velocity  $\vec{V}$  of the free boundary  $\Gamma$  is given by

$$\vec{V}(\vec{x}, t) = \lambda(-D_s \vec{\nabla} s \cdot \hat{\nu} + s \chi \hat{x} \cdot \hat{\nu}) \hat{\nu} \quad \text{on} \quad \Gamma(t) \quad (6)$$

that reduces to

$$\vec{V}(\vec{x}, t) = -(\lambda D_s \vec{\nabla} s \cdot \hat{\nu}) \hat{\nu} \quad \text{on} \quad \Gamma(t) \quad (7)$$



as we prescribed  $s(\vec{x}, t) = 0$  on  $\Gamma$  (Eq. (5)). The velocity is proportional to the stem cell gradient on  $\Gamma$ . The parameter  $\lambda$  represents essentially the volume of a single myocardial cell, averaged by the probability that a stem cell arriving at  $\Gamma$  differentiates into such a cell.

In a more refined model the link between  $\vec{V}$  and  $s$  could not be as simple as in (7); however, the velocity of the interface should still be prescribed as a function of the local flux of differentiated stem cells. The latter flux, though, should be determined by a reaction-diffusion system controlling differentiation.

Summarizing, the free boundary problem (Eq.s (1) to (5) and Eq. (7)) describing the stem cell dynamics is given by

$$\left\{ \begin{array}{ll} \frac{\partial s}{\partial t} - \operatorname{div} \left( D_s \vec{\nabla} s - s \chi \hat{x} \right) = \mu_{max} \frac{n(1+K)}{n_{max}K+n} s \left( 1 - \frac{s}{s_{max}} \right) - R_d s & D(t), t \in (0, T) \\ s(\vec{x}, 0) = 0 & D(0) \\ s(\vec{x}, t) = BC(t) & A \times (0, T) \\ \frac{\partial s}{\partial \hat{\nu}}(\vec{x}, t) = 0 & (\partial E \setminus A) \times (0, T) \\ s(\vec{x}, t) = 0 & \Gamma(t), t \in (0, T) \\ \vec{V}(\vec{x}, t) = -(\lambda D_s \vec{\nabla} s \cdot \hat{\nu}) \hat{\nu} & \Gamma(t), t \in (0, T) \end{array} \right. \quad (8)$$

## 2.2 Nutrient dynamics

The dynamics of the nutrient in  $D$  over the interval of time  $[0, T]$  is governed by the following diffusion-reaction equation:

$$\frac{\partial n}{\partial t} - \operatorname{div} \left( D_n \vec{\nabla} n \right) = -\delta_{max} \frac{n^4}{\vartheta^4 + n^4} s. \quad (9)$$

The diffusion term describes the spread of nutrients in the tissue. Considering the values reported in the literature [58–61], and taking into account that the molecules can move more rapidly than cells, the diffusion coefficient  $D_n$  can be set at least an order of magnitude higher than the diffusion coefficients of the stem cells. The reaction term describes the nutrient consumption depending on the stem cell concentration. To describe the consumption rate we decided to use a Hill function with exponent 4 and constant  $\vartheta$ , where the parameter  $\delta_{max}$  is the maximum consumption rate [62]. The Hill function typically describes cooperative phenomena in enzyme kinetic, but is used

also in models considering higher organisms [63]. The exponent (in this case 4) is in general deduced from experimental data and governs the steepness of the sigmoidal shape of the saturation term. In our model, in absence of experimental data, we arbitrarily decided to set the coefficient equal to 4.

Equation (9) is supplemented by initial and boundary conditions, as follows. A constant initial condition is set on the domain  $D(0)$ :

$$n(\vec{x}, 0) = n_0 \quad \text{on} \quad D(0)$$

where  $n_0$  is the nutrient concentration at the beginning of the process. A Neumann boundary condition is imposed on  $\Gamma$ , as we assume that nutrients do not permeate inside the necrotic core:

$$D_n \vec{\nabla} n \cdot \hat{\nu} = 0 \quad \text{on} \quad \Gamma. \quad (10)$$

Finally, a condition on the flux through the entire external boundary  $\partial E$  is prescribed:

$$D_n \vec{\nabla} n \cdot \hat{\nu} = F(n) \quad \text{on} \quad \partial E. \quad (11)$$

We make two possible choices for the function  $F$ . The first one is to define  $F(n) \equiv 0$  that corresponds to imposing a null Neumann condition:

$$D_n \vec{\nabla} n \cdot \hat{\nu} = 0 \quad \text{on} \quad \partial E. \quad (12)$$

In this case we assume that stem cells feed on the nutrient initially available in the domain. The second choice is to define  $F(n) = -H(n - n_0)$ , where  $H$  is a positive constant. The resulting condition

$$D_n \vec{\nabla} n \cdot \hat{\nu} = -H(n - n_0) \quad \text{on} \quad \partial E \quad (13)$$

prescribes an inward flux<sup>1</sup> if the concentration decreases below  $n_0$  ( $n < n_0$ ) and an outward flux if  $n$  exceeds the initial concentration ( $n > n_0$ ). Due to this condition, additional nutrient is attracted from outside when the nutrient is consumed by the stem cells in the domain, thus simulating the effects of the angiogenesis promoted by the presence of the stem cells in the tissue.

---

<sup>1</sup>Note the change of sign in (13): the lhs is the incoming flux, so it must be positive if  $n < n_0$ .

Summarizing, the initial-boundary value problem for the diffusion-reaction equation describing the nutrients dynamics (Eq.s (9) to (11)) is given by

$$\begin{cases} \frac{\partial n}{\partial t} - \operatorname{div} \left( D_n \vec{\nabla} n \right) = -\delta_{max} \frac{n^4}{\vartheta^4 + n^4} s & D(t), t \in (0, T) \\ n(\vec{x}, 0) = n_0 & D(0) \\ D_n \vec{\nabla} n \cdot \hat{\nu} = 0 & \Gamma(t), t \in (0, T) \\ D_n \vec{\nabla} n \cdot \hat{\nu} = F(n) & \partial E \times (0, T) \end{cases} \quad (14)$$

where  $F(n)$  is given by Eq. (12) or Eq. (13).

### 3 Methods

The two differential problems have been non-dimensionalized with respect to the concentrations by posing

$$s = s_{max} \bar{s}, \quad n = n_{max} \bar{n}, \quad \vartheta = n_{max} \bar{\vartheta} \quad (15)$$

so that the new non-dimensional variables  $\bar{s}$  and  $\bar{n}$  are normalized to the reference values  $s_{max}$  and  $n_{max}$ . The systems of equations and the initial and boundary conditions can be rewritten as

$$\begin{cases} \frac{\partial \bar{s}}{\partial t} - \operatorname{div} \left( D_s \vec{\nabla} \bar{s} - \bar{s} \chi \hat{x} \right) = \mu_{max} \frac{\bar{n}(1+K)}{K+\bar{n}} \bar{s} (1 - \bar{s}) - R_d \bar{s} & D(t), t \in (0, T) \\ \bar{s}(\vec{x}, 0) = 0 & D(0) \\ \bar{s}(\vec{x}, t) = \overline{BC}(t) & A \times (0, T) \\ \frac{\partial \bar{s}}{\partial \bar{\nu}}(\vec{x}, t) = 0 & (\partial E \setminus A) \times (0, T) \\ \bar{s}(\vec{x}, t) = 0 & \Gamma(t), t \in (0, T) \\ \vec{V}(\vec{x}, t) = -(\lambda D_s s_{max} \vec{\nabla} \bar{s} \cdot \hat{\nu}) \hat{\nu} & \Gamma(t), t \in (0, T) \end{cases} \quad (16)$$

$$\begin{cases} \frac{\partial \bar{n}}{\partial t} - \operatorname{div} \left( D_n \vec{\nabla} \bar{n} \right) = -\delta \frac{\bar{n}^4}{\bar{\vartheta}^4 + \bar{n}^4} \bar{s} & D(t), t \in (0, T) \\ \bar{n}(\vec{x}, 0) = \bar{n}_0 & D(0) \\ D_n \vec{\nabla} \bar{n} \cdot \hat{\nu} = 0 & \Gamma(t), t \in (0, T) \\ D_n \vec{\nabla} \bar{n} \cdot \hat{\nu} = F(\bar{n}) & \partial E \times (0, T) \end{cases} \quad (17)$$

where  $\overline{BC}$  is the smoothed decreasing step function from  $\bar{s}_0 = \frac{s_0}{s_{max}}$  to 0,  $\delta = \frac{\delta_{max} s_{max}}{n_{max}}$ ,  $\bar{n}_0 = \frac{n_0}{n_{max}}$  and  $F(\bar{n}) \equiv 0$  or  $F(\bar{n}) = -H(\bar{n} - \bar{n}_0)$ .

The model has been implemented in the software COMSOL Multiphysics<sup>®</sup> that is an integrated environment for solving systems of time-dependent or stationary differential problems in one, two, and three dimensions with Finite Element Method [64].

Comsol Multiphysics<sup>®</sup> provides sophisticated tools for geometric modeling of the physical domain. The simulations have been performed on the 3D geometry depicted in Figure 1. The semi-axes of the external and internal ellipsoids are  $a_{ext}$ ,  $b_{ext}$ ,  $c_{ext}$  and  $a_{int}$ ,  $b_{int}$ ,  $c_{int}$ , respectively. The implantation site  $A$  has been obtained by the intersection of the external ellipsoid with a sphere of radius  $r_{imp}$  and position  $(a_{ext} \cos(\pi/4), 0, c_{ext} \sin(\pi/4))$ .

The software also offers different methods and levels of domain tassellation. In order to obtain a well detailed solution, we chose the tetrahedral mesh at the highest level of mesh resolution, that is “Extremely fine” (Figure 2). Complete mesh consists of 343239 domain elements and 13476 boundary elements with maximum element size  $4 \cdot 10^{-4} m$ , minimum element size  $4 \cdot 10^{-6} m$  and maximum element growth rate 1.3.

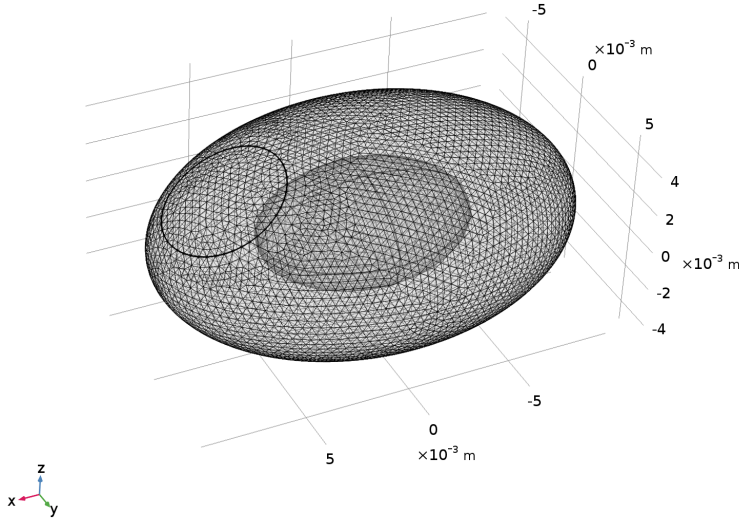


Figure 2: Mesh of the domain  $D$  with tetrahedral elements. The “Extremely fine” mesh resolution level results in 343239 domain elements and 13476 boundary elements.

The numerical solution gives the cell concentration  $s(x, t)$  at each mesh point after each time unit. Many direct and iterative methods are available in the software to evaluate the numerical solution. The problem has been

solved with the direct solver MUMPS (multifrontal massively parallel sparse direct solver) with relative tolerance 0.01 and absolute tolerance 0.001 [65]. Although direct methods require more memory and computational time than iterative methods, they are more robust. Among them, the MUMPS solver is more suitable for problems that have a large number of degrees of freedom. The implicit time stepping method used by the solver is the Backward Differentiation Formula (BDF) with order of accuracy from 1 to 5.

Since in our study we intend to investigate the possibility of describing some qualitative aspects of the therapy through differential problems, our actual aim is not to validate the model with experimental data, which, however, are in general difficult to be determined. The parameters used in the model have been chosen in accordance with what is known in the literature on the aspects we are describing. Their choice is purely indicative but still reasonable and compatible with known physiological values. Some of them depend on the cell type and nutrient type. As we did not consider a particular real situation, we fixed them in physiologically reliable ranges. For the cell dynamics we referred in particular to the parameters related to mesenchymal stem cells; for the nutrient dynamics we referred in particular to the parameters related to oxygen [50, 54, 66–70]. See Table 2 for the complete list of the parameters used in the simulations, their value and unit.

The non-dimensionalized boundary condition  $\overline{BC}(t)$  prescribed on the implantation site  $A$  is shown in Figure 3. The initial stem cell concentration in each point of  $A$  rapidly decreases to 0 within the first half hour of the experiment and remains null thereafter.

Parameter	Description	Value	Unit
$a_{ext}$	$x$ semi-axis of external ellipsoid	$1 \cdot 10^{-2}$	$[m]$
$b_{ext}$	$y$ semi-axis of external ellipsoid	$7 \cdot 10^{-3}$	$[m]$
$c_{ext}$	$z$ semi-axis of external ellipsoid	$5 \cdot 10^{-3}$	$[m]$
$a_{int}$	$x$ semi-axis of internal ellipsoid	$5 \cdot 10^{-3}$	$[m]$
$b_{int}$	$y$ semi-axis of internal ellipsoid	$3.5 \cdot 10^{-3}$	$[m]$
$c_{int}$	$z$ semi-axis of internal ellipsoid	$2.5 \cdot 10^{-3}$	$[m]$
$r_{imp}$	Radius of the sphere that defines the im- plantation site	$3 \cdot 10^{-3}$	$[m]$
$D_s$	Stem cell diffusion coefficient	$2 \cdot 10^{-12}$	$[m^2/s]$
$\chi$	Sensitivity of the stem cells to chemoat- traction	$8 \cdot 10^{-9}$	$[m/s]$
$\mu_{max}$	Maximum proliferation rate	$1 \cdot 10^{-5}$	$[1/s]$
$n_{max}$	Maximum nutrient concentration in the tissue	$8 \cdot 10^{-2}$	$[mol/m^3]$
$s_{max}$	Maximum cell concentration in the tissue	$1 \cdot 10^{12}$	$[1/m^3]$
$K$	Half saturation constant	$5 \cdot 10^{-2}$	$[1]$
$R_d$	Stem cell death rate	$3 \cdot 10^{-7}$	$[1/s]$
$s_0$	Initial stem cell concentration on the im- plantation site	$1 \cdot 10^{12}$	$[1/m^3]$
$\lambda$	Cell volume conversion factor	$1 \cdot 10^{-9}$	$[m^3]$
$D_n$	Nutrient diffusion coefficient	$2 \cdot 10^{-11}$	$[m^2/s]$
$\delta_{max}$	Maximum nutrient consumption rate	$8 \cdot 10^{-16}$	$[mol/s]$
$\vartheta$	Hill function constant	$4 \cdot 10^{-2}$	$[mol/m^3]$
$n_0$	Initial nutrient concentration in the do- main	$4 \cdot 10^{-2}$	$[mol/m^3]$
$H$	Proportionality constant in the nutrient flux	$1 \cdot 10^{-2}$	$[m/s]$
$T$	Duration of the experiment	96	$[h]$

Table 2: List of the parameters used in the simulations, their description, numerical value and unit.

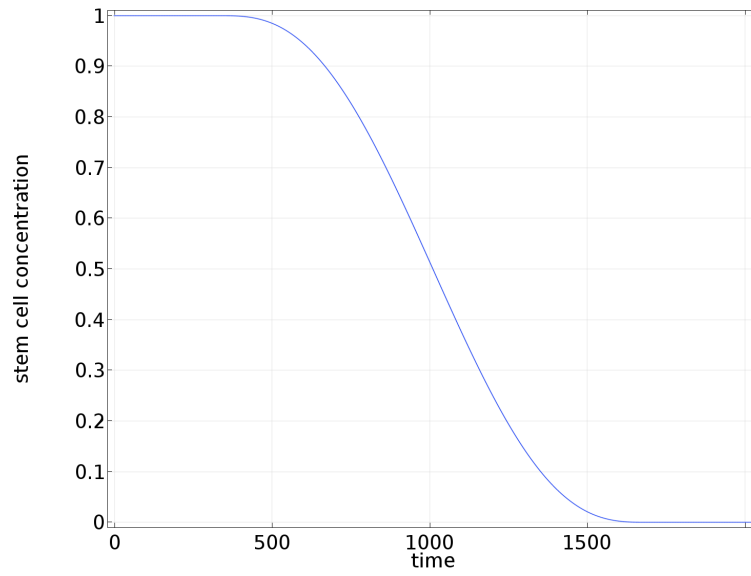


Figure 3: Non-dimensionalized boundary condition  $\overline{BC}(t)$  prescribed on  $A$  (Eq.(3)). It defines the stem cell concentration in each point of  $A$  during time. It is a decreasing step function from 1 to 0 with a smooth transition zone covering about the first half hour of the experiment. It remains 0 out of that interval of time.

## 4 Results

Two different cases have been considered in the simulations, according to the definition of the function  $F$  that prescribes the flux of nutrients across the external boundary.

As a first experiment we focus on stem cell dynamics. We are interested in observing how diffusion combined with chemoattraction causes cells to move and reach the boundary of the necrotic zone. Through the simulation we are able to follow the trajectories of the cells by observing their concentration in the tissue. The quantity of cells arriving on the boundary and their arrangement around the necrotic zone makes us appreciate the progressive deformation of the domain, confirming the model's ability to describe this aspect. Nutrient consumption is present but is limited only to the amount of nutrient initially present in the domain. Proliferation is also present, and is proportionate to that quantity.

To test the potential of the coupling between the dynamics of cells and nutrients, in a second experiment we also consider how the supply of new nutrients modifies the dynamics of stem cells, all other conditions being equal. We then add a flow of nutrients from the outside. Through the simulation we can observe how the model reacts to a non-static condition of nutrients, apart from the diffusion. In this way we can simulate the effect of angiogenesis in view of a more detailed model of the formation of new blood vessels. The results confirm us in the prediction of a greater proliferation and consequent greater recovery of the necrotic area, underlining the importance of the interaction between the two differential systems.

These preliminary experiments confirm the model's ability to describe the therapy in different situations. Other experiments could be done by changing the boundary conditions or parameters values. For example, other boundary conditions could be defined that describe stem cell implantation to simulate different cell delivery protocols (not shown here). In any case, the model turns out to be a versatile tool capable of adapting to fit the desired aspects of the therapy.

### 4.1 Experiment 1

In the first experiment, the Neumann boundary condition for the nutrient flux  $D_n \vec{\nabla} n \cdot \hat{\nu} = 0$  is prescribed on the external boundary  $\partial D$  in the system (17). Stem cell and nutrient concentrations evolve according to Eq.s (16) and (17)



in the time interval  $[0, T]$ . A 3D representation of the non-dimensionalized stem cell concentration dynamics is shown in Figure 4. The values of the concentration are represented through five iso-surfaces from  $0.15 \cdot 10^{-4}$  to  $5 \cdot 10^{-4}$  after 4, 24, 48, 64, 80 and 96 hours. To better appreciate the time evolution of the stem cell concentration and the tissue regeneration, the same sequence is shown on the  $xz$  section plane through a continuous color range from 0 to  $1 \cdot 10^{-3}$  in Figure 5. The simultaneous non-dimensionalized nutrient concentration dynamics is shown in Figure 6. The nutrient concentration is represented on the same  $xz$  plane through a continuous color range from 0.36 to 0.5 in the same instants of time.

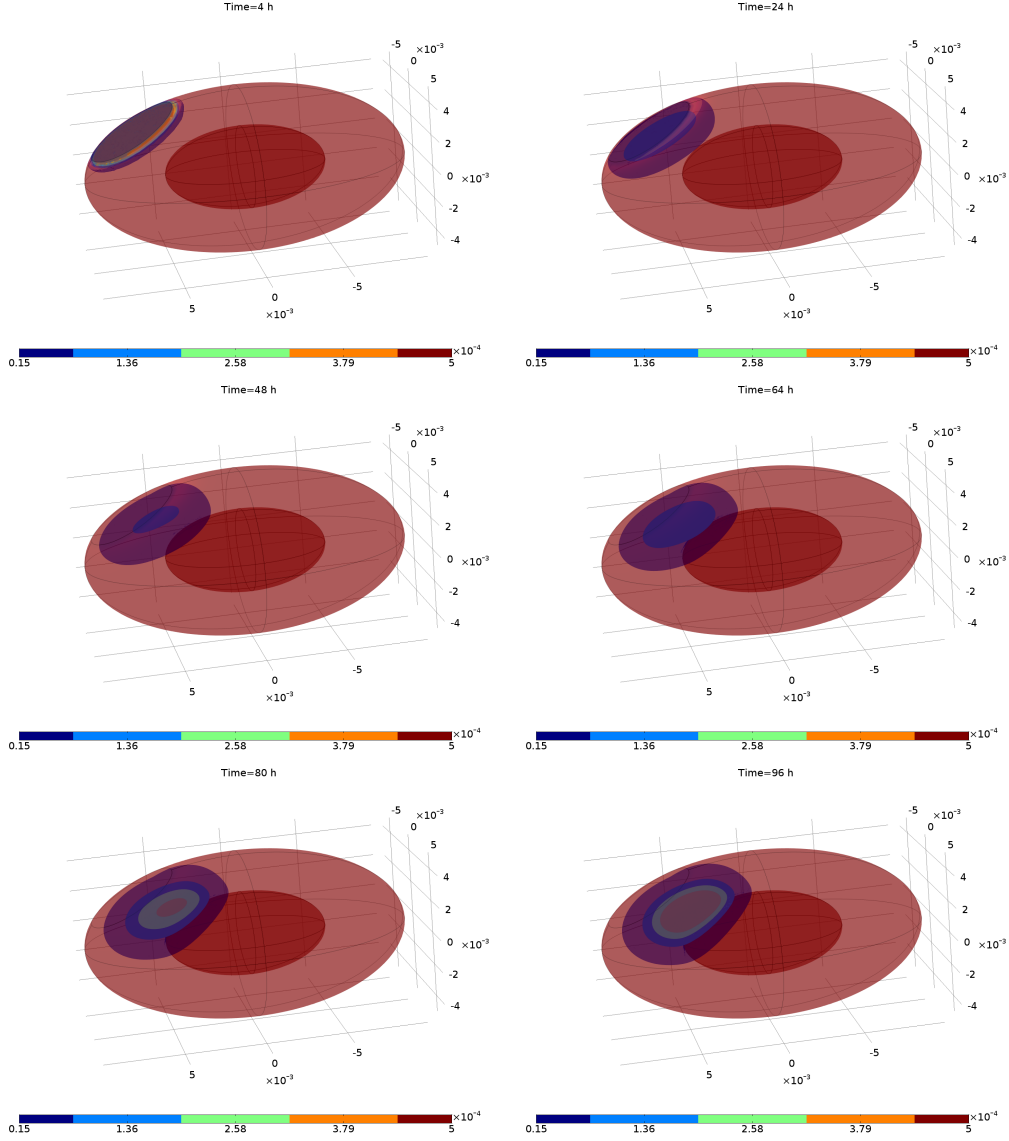


Figure 4: Experiment 1: 3D representation of the non-dimensionalized stem cell concentration in the domain  $D$  during time. The concentration is represented through five iso-surfaces of different colors on a fixed scale from  $0.15 \cdot 10^{-4}$  to  $5 \cdot 10^{-4}$ . The panels from left to right, from top to bottom, show the cell concentration in a sequence of 6 instants of time: after 4, 24, 48, 64, 80, 96 hours from the beginning of the experiment.

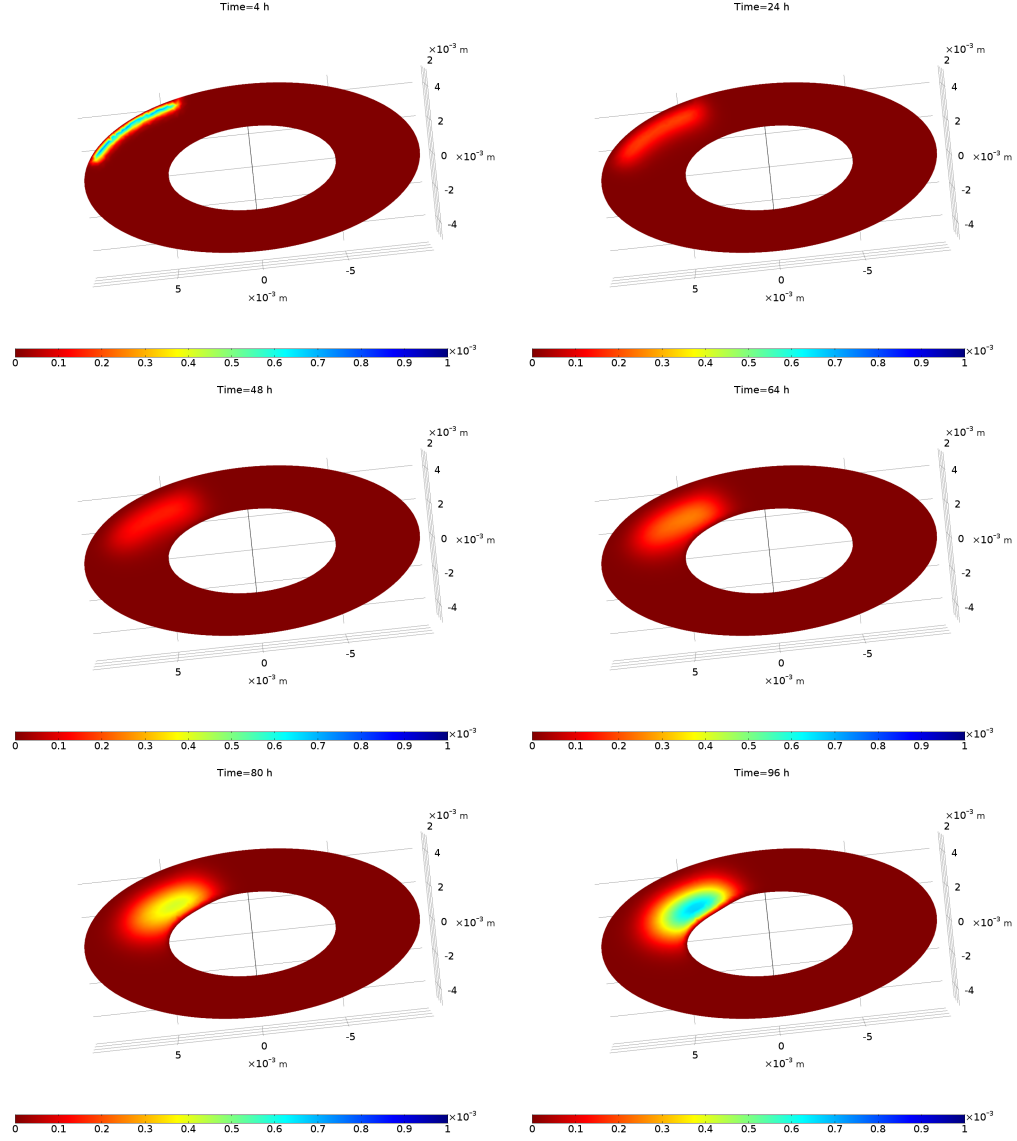


Figure 5: Experiment 1: non-dimensionalized stem cell concentration on the  $xz$  section plane of the domain  $D$  during time. The concentration is represented through a continuous color range from dark red to dark blue on a fixed scale from 0 to  $1 \cdot 10^{-3}$ . The panels from left to right, from top to bottom, show the cell concentration in a sequence of 6 instants of time: after 4, 24, 48, 64, 80, 96 hours from the beginning of the experiment.

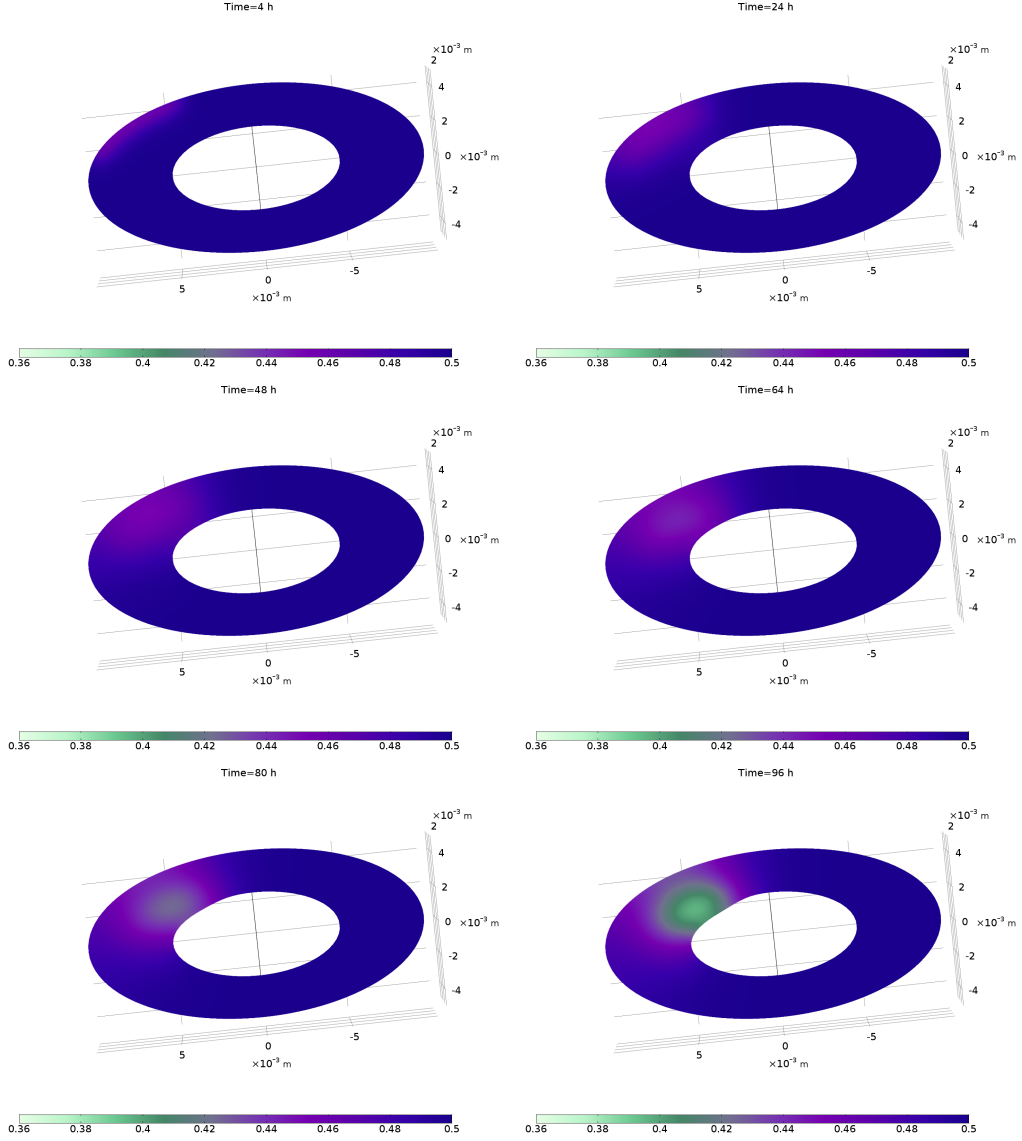


Figure 6: Experiment 1: non-dimensionalized nutrient concentration on the  $xz$  section plane of the domain  $D$  during time. The concentration is represented through a continuous color range from white to dark purple on a fixed scale from 0.36 to 0.5. The panels from left to right, from top to bottom, show the cell concentration in a sequence of 6 instants of time: after 4, 24, 48, 64, 80, 96 hours from the beginning of the experiment.

The profile of the stem cell concentration along a suitable cut line can also give a quantitative idea of the shrinking of the necrotic core at the end of the experiment due to an increasing gradient of the concentration on the internal boundary  $\Gamma$ . Let us consider the segment  $\gamma$  connecting the center of the implantation region  $A$  on the external boundary  $\partial E$  with the boundary  $\Gamma$  of the necrotic core along the radial direction (Figure 7). Figure 8 shows the same sequence of the stem cell concentration restricted to the considered segment  $\gamma$  versus the arc length that changes over time.

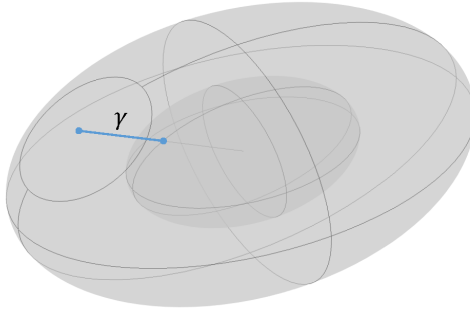


Figure 7: Cut line  $\gamma$  along which we follow the evolution of the stem cell concentration in Experiment 1 (see Figure 8).  $\gamma$  is the segment connecting the center of the implantation region  $A$  on the external boundary  $\partial E$  with the boundary  $\Gamma$  of the necrotic core along the radial direction. Its length changes over time according to the domain deformation.

## 4.2 Experiment 2

In the second experiment, the condition for the nutrient flux  $D_n \vec{\nabla} \bar{n} \cdot \hat{\nu} = -H(\bar{n} - \bar{n}_0)$  is prescribed on the external boundary  $\partial D$  in the system (17). The non-dimensionalized stem cell and nutrient concentrations dynamics are shown in Figure 9 and Figure 10, respectively, in the  $xz$  plane representation. The instants of time and the color ranges of the sequences are intentionally kept the same as in Experiment 1, in order to allow a direct comparison of the results.

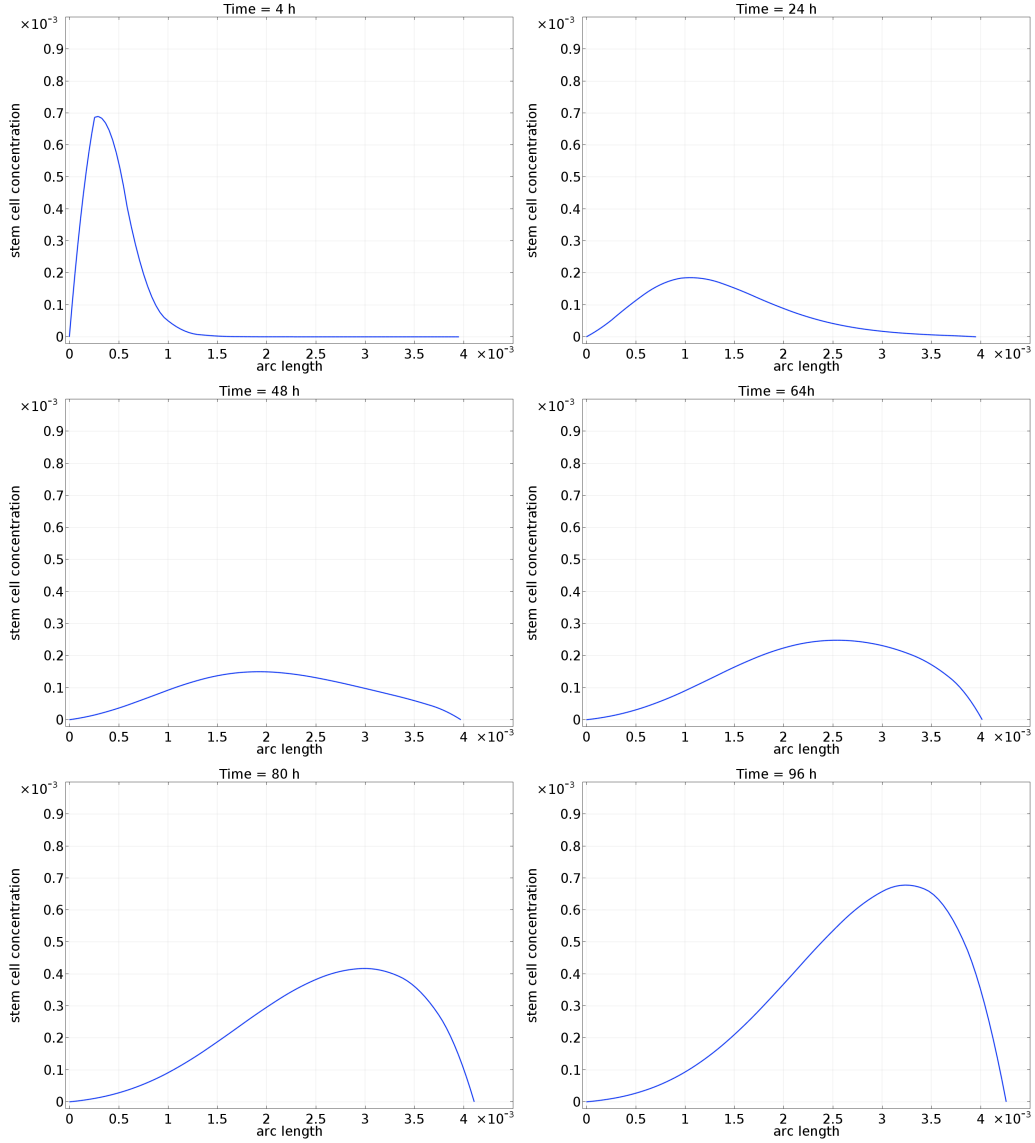


Figure 8: Experiment 1: non-dimensionalized stem cell concentration on the points of the cut line  $\gamma$  (see Figure 7) during time. The panels from left to right, from top to bottom, show the cell concentration in a sequence of 6 instants of time: after 4, 24, 48, 64, 80, 96 hours from the beginning of the experiment. The origin of the arc length on the horizontal axis coincides with the central point of the stem cell implantation site  $A$ . The other extreme of the segment lying on the internal boundary moves right according to the domain deformation resulting in a final elongation of the segment (compare the last panel with the first one).

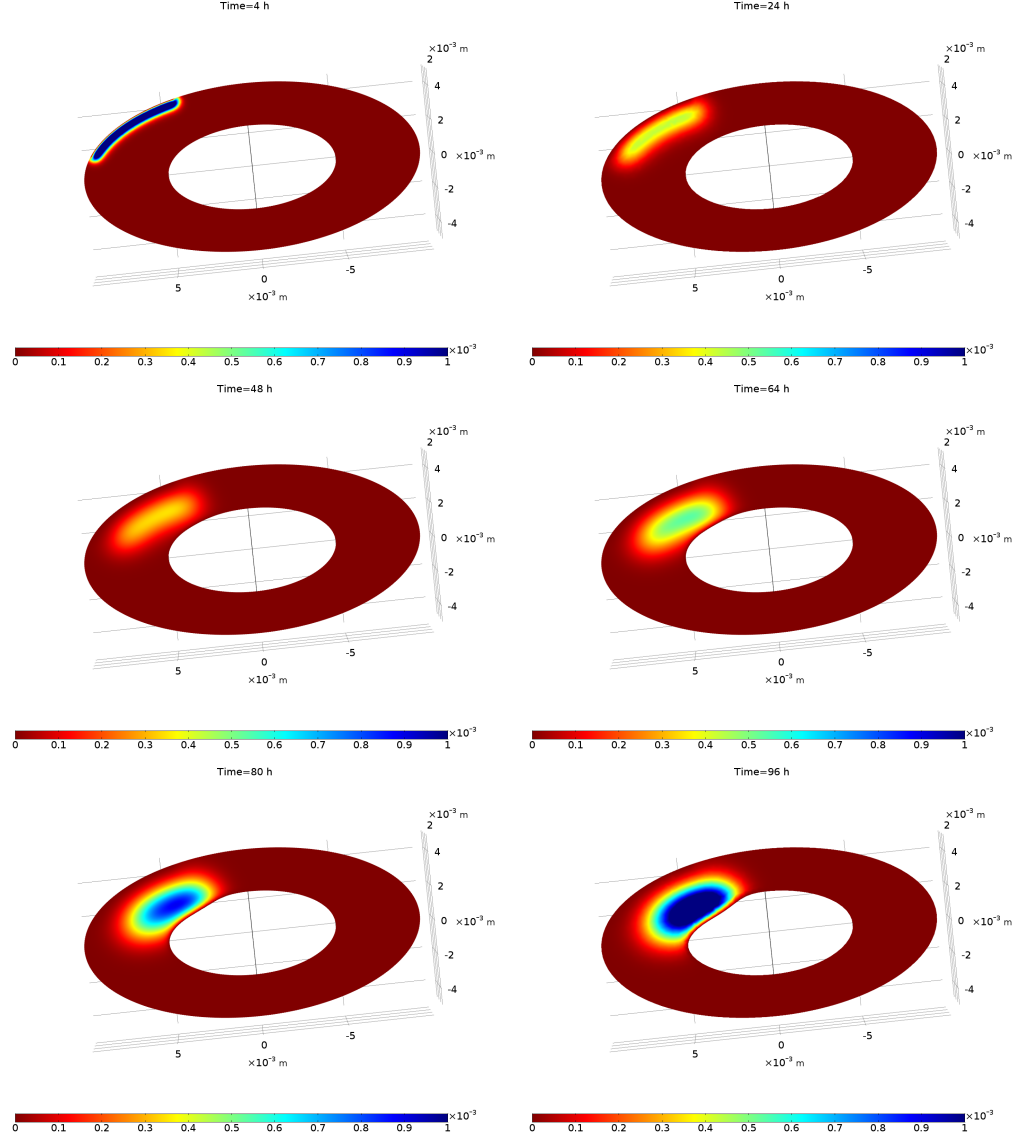
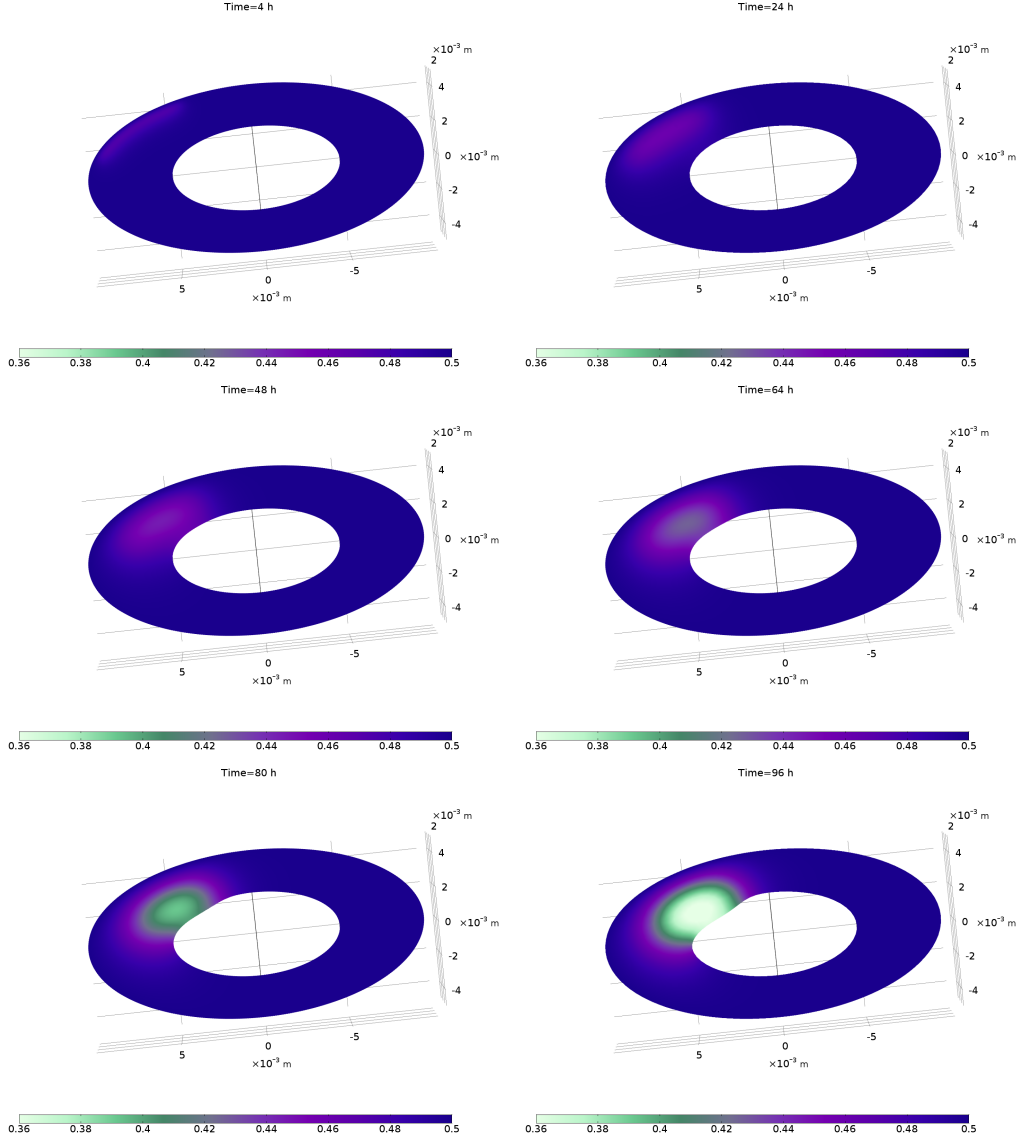


Figure 9: Experiment 2: non-dimensionalized stem cell concentration on the  $xz$  section plane of the domain  $D$  during time. The concentration is represented through a continuous color range from dark red to dark blue on a fixed scale from 0 to  $1 \cdot 10^{-3}$ . The panels from left to right, from top to bottom, show the cell concentration in a sequence of 6 instants of time: after 4, 24, 48, 64, 80, 96 hours from the beginning of the experiment. The dark blue points correspond to a concentration higher or equal to the maximum of the scale.





### 4.3 Results description

The results of the simulations show the expected qualitative behavior of the system. Referring to the first experiment, the stem cells diffuse in the domain starting from the site of implantation and move toward the necrotic core due to chemoattraction (see the sequence in Figure 4). As a consequence, the initial peak in the concentration near the implantation zone gradually decreases as the stem cells spread around in the tissue (see the results in Figure 5 after 4, 24 and 48 hours). Thereafter, as cells thicken around the necrotic zone and due to their proliferation, the concentration rises again around the boundary of the necrotic core. When the concentration gradient gets high enough, the boundary begins to move and the necrotic core begins to contract. The shrinking of the necrotic core is slightly visible after 64 hours and becomes more evident after 80 and 96 hours.

During the entire process, stem cells feed on the nutrient that is already present in the domain. The light areas in Figure 6 indicate the decrease in nutrients with respect to the initial value due to the passage of the stem cells. At the end of the experiment, a lighter area is observed in correspondence with the points where there is the greatest concentration of stem cells, and hence a greater nutrient consumption. The different shapes of the areas where the nutrient is consumed with respect to the actual location of the stem cells and their smoothed edges are due to the nutrient faster diffusion (compare Figure 5 and 6 at the same instants of time).

The functioning underlying the process can be better appreciated by following the concentration profile along the cut line  $\gamma$  (Figure 8). The peak in concentration is initially close to the left extreme of the segment that coincides with the origin of the arc length on the horizontal axes in Figure 8. It gradually decreases over time moving to the opposite extreme and then rises again after about half of the experiment. The increase in the extent of the area under the graph reveals an increase in the cell population due to proliferation. Condition (5) makes the concentration always be zero on the second extreme of the segment lying on  $\Gamma$ . The increasing in the absolute value of the slope of the graph in that point causes the movement to the right of the extreme. As a consequence, the segment stretches during the process since the cells begin to thicken around the extreme. The initial arc length is  $3.99 \cdot 10^{-3} m$ . It starts increasing at about the middle of the experiment and its final value after 96 hours is  $4.30 \cdot 10^{-3} m$ . The elongation  $3.10 \cdot 10^{-4} m$  indicates the amount of regenerated tissue along the radial direction at the

end of the experiment.

In the second experiment, a nutrient flux from outside is allowed whenever the concentration inside the domain decreases. The behavior of the system is similar to that observed in the first experiment, but some remarkable differences have to be highlighted. Comparing the stem cell concentration in the same instants of time (Figures 5 and 9) we find out that the concentration is higher in the second experiment. At 96 hours the peak exceeds the fixed threshold of the color range used for the representation in a fairly large area close to the necrotic core, while in the first experiment that threshold is never reached. Furthermore, a much more marked narrowing of the necrotic area is observable at the end of the second experiment. In fact, the supply of nutrients from outside promotes cell proliferation and a higher number of cells reaching the necrotic area promotes tissue regeneration.

The nutrient dynamics is also different in the two cases. In the first experiment the consumption area, that corresponds to the light zones in Figure 6, covers all the points occupied by the stem cells during the whole process, from the implantation site to the necrotic core. In fact in this case the nutrient is only consumed by the stem cells and diffuses. The blurring of the edges and the smoothing of the values are the effect of the diffusion. In the second experiment, instead, additive nutrients enter the domain from the external boundary. This effect is mainly visible in the area close to the implantation site that remains dark over time, indicating a high nutrient concentration due to the additional flow (Figure 10). But if on the one hand the nutrients attracted from the outside compensate the consumption of the nutrient in the domain, on the other hand they favor the growth of the cell population and therefore the consumption of nutrient itself. At the end of the experiment a greater consumption is observed in the area near the necrotic core (a greater light area) due to the greater number of cells that have arrived in that zone compared to the first experiment.

## 5 Discussion and conclusion

In this paper we have proposed a 3D model describing stem cell and nutrient dynamics in a heart tissue regenerative therapy through two coupled differential problems. We analysed the potential of the mathematical tools used in the model in describing some fundamental aspects of the therapy. We analysed the functioning of the model by performing the simulations in two

different situations, where we tested how the supply of new nutrients modifies the dynamics of stem cells, all other conditions being equal. The results show the importance of the nutrient supply. This implies that, in particular, the angiogenesis must be inserted in future developments of the model, in order to guarantee the nutrient supply to the regenerated tissue.

Clearly, the model has many limitations, since we made some simplifications and arbitrary assumptions, as previously discussed. Moreover we did not consider the effects of cardiac muscle movement during the heartbeat.

The model could be improved in various ways. Some ameliorations include: considering a different geometry of the spatial domain; defining a more accurate diffusion term that accounts for the 3D motion of the cells and nutrients in the cardiac tissue [71–74]; coupling the model with a differential problem describing the dynamics of chemokines for a more reliable description of chemoattraction; distinguishing the different stages of cell maturation after their engraftment and different kinds of nutrients; modeling the angiogenesis [75–80], just to list a few.

For a comprehensive description of all the processes involved in such a complex biological framework, a multiscale approach should be adopted, capable of capturing the mechanisms that occur at inter-cellular, intra-cellular and cell populations scales [19]. At present this task is challenging, due to the number and complexity of the mechanisms that have to be accounted for, some of which have not yet been fully clarified. But even in simplified schemes, mathematical models and simulations can help observing, characterizing and predicting natural processes, thus offering valid tools to consolidate knowledge and shed more light on aspects that are not yet known.

Moreover, in biological models, stochastic effects should be in general taken into consideration. For example, it is well known that the fate decision of stem cells, as for all cells, is affected by stochastic events (see, for example [81,82]), at the intracellular level in terms of signal transduction network, or of the genetic and epigenetic networks.

Furthermore, while at inter-cellular level the application of diffusion equations is the natural simplification of the stochastic nature of diffusion phenomena, stochastic effects due to fluctuations of environmental cues, which influence the fate (proliferation/differentiation) of the cells can also be considered (see, for example, [19]). Models at this mesoscopical level (extracellular) have been formulated (see, for example, [83,84]). For nice review works, see [85–87]. In a future version of our model, we will tackle these facets of the process.

The model follows the stem cells from the part  $A$  of the boundary  $\partial E$ , to the boundary of the necrotic core, where they replace the necrotic cells with regenerated tissue. On the one hand, in the future we can take into consideration different protocols by which the stem cells arrive at the boundary of the inflamed zone, for example adjusting the boundary conditions. On the other hand, the module describing the growth of the regenerated tissue must be expanded, leading to the coupling of the law for the growth rate of  $\Gamma(t)$  with the local cascade of differentiation, which in principle may depend on many chemical and physical factors (see, for example, [19, 27, 28]).

However, such improvements of the model will clearly imply the need of much more detailed experimental data (which are, in general, difficult to be determined in the literature), besides increasing the mathematical complexity.

## References

- [1] Doppler SA, Deutsch MA, Lange R, Krane M. Cardiac regeneration: current therapies-future concepts. *Journal of Thoracic Disease*, 5 (5): 683–697, 2013. doi: 10.3978/j.issn.2072-1439.2013.08.71.
- [2] Arbatlı S, Aslan GS, Kocabaş F. Stem Cells in Regenerative Cardiology. *Advances in Experimental Medicine and Biology*, 1079: 37–53, 2018. doi: 10.1007/5584\_2017\_113.
- [3] Sanganalmath SK, Bolli R. Cell therapy for heart failure: a comprehensive overview of experimental and clinical studies, current challenges, and future directions. *Circulation Research*, 113 (6): 810–34, 2013. doi: 10.1161/CIRCRESAHA.113.300219.
- [4] Sun R, Li X, Liu M, Zeng Y, Chen S, Zhang P. Advances in stem cell therapy for cardiovascular disease (Review). *International Journal of Molecular Medicine*, 38 (1): 23–29, 2016. doi:10.3892/ijmm.2016.2607.
- [5] Leri A, Kajstura J, Anversa P. Mechanisms of myocardial regeneration. *Trends in Cardiovascular Medicine*, 21 (2): 52–58, 2011. doi:10.1016/j.tcm.2012.02.006.
- [6] Müller P, Lemcke H, David R. Stem Cell Therapy in Heart Diseases - Cell Types, Mechanisms and Improvement Strategies. *Cellular Physiology and Biochemistry*, 48 (6): 2607–2655, 2018. doi: 10.1159/000492704.

- [7] Gnecchi M., Cervio E. (2013) Mesenchymal Stem Cell Therapy for Heart Disease. In: Chase L., Vemuri M. (eds) Mesenchymal Stem Cell Therapy. Stem Cell Biology and Regenerative Medicine. Humana Press, Totowa, NJ. [https://doi.org/10.1007/978-1-62703-200-1\\_13](https://doi.org/10.1007/978-1-62703-200-1_13).
- [8] Bernal A, Gálvez BG. The Potential of Stem Cells in the Treatment of Cardiovascular Diseases. *Stem Cell Reviews and Reports*, 9: 814–832, 2013.
- [9] Ferraris A. How do cells talk to each other?: Paracrine factors secreted by mesenchymal stromal cells. *The Journal of Thoracic and Cardiovascular Surgery*, 151 (3): 849–851, 2016.
- [10] Madonna R (eds). *Stem Cells and Cardiac Regeneration*. Stem Cell Biology and Regenerative Medicine Series, Springer International Publishing Switzerland, 2016. ISBN: 978-3-319-25425-8.
- [11] Gnecchi M, Zhang Z, Ni A, Dzau VJ. Paracrine mechanisms in adult stem cell signaling and therapy. *Circulation Research*, 103 (11): 1204–1219, 2008. doi: 10.1161/CIRCRESAHA.108.176826.
- [12] Chen B, Frangogiannis NG. Chemokines in Myocardial Infarction. *Journal of cardiovascular translational research*, 14 (1): 35–52. doi: 10.1007/s12265-020-10006-7.
- [13] Karpov AA, Udalova DV, Pliss MG, Galagudza MM. Can the outcomes of mesenchymal stem cell-based therapy for myocardial infarction be improved? Providing weapons and armour to cells. *Cell Proliferation*, 50 (2): e12316, 2017. doi:10.1111/cpr.12316.
- [14] Penn MS (eds). *Stem Cells and Myocardial Regeneration*. Contemporary Cardiology Series, Humana Press, 2007. ISBN: 978-1-59745-272-4.
- [15] Wu KH, Han ZC, Mo XM, Zhou B. Cell delivery in cardiac regenerative therapy. *Ageing Research Reviews*, 11 (1): 32–40, 2012. doi: 10.1016/j.arr.2011.06.002.
- [16] Prat-Vidal C, Rodríguez-Gómez L, Aylagas M, Nieto-Nicolau N, Gastelurrutia P, Agustí E, Gálvez-Montón C, Jorba I, Teis A, Mongui-Tortajada M, Roura S, Vives J, Torrents-Zapata S, Coca MI, Reales L, Cámara-Rosell ML, Cedié G, Coll R, Farré R, Navajas D, Vilarrodona A, García-López J, Muñoz-Guijosa C, Querol S, Bayes-Genis A. First-in-human PeriCord cardiac bioimplant: Scalability and GMP manufacturing of an allogeneic engineered tissue graft. *EBioMedicine*, 54: 102729, 2020. doi: 10.1016/j.ebiom.2020.102729.

- [17] Kollar K, Cook MM, Atkinson K, Brooke G. Molecular mechanisms involved in mesenchymal stem cell migration to the site of acute myocardial infarction. *International Journal of Cell Biology*, 2009: 904682, 2009. doi: 10.1155/2009/904682.
- [18] Li L, Jiang J. Regulatory factors of mesenchymal stem cell migration into injured tissues and their signal transduction mechanisms. *Frontiers of Medicine*, 5 (1): 33–39, 2011. doi: 10.1007/s11684-011-0114-1.
- [19] Wadkin LE, Orozco-Fuentes S, Neganova I, Lako M, Shukurov A, Parker NG. The recent advances in the mathematical modelling of human pluripotent stem cells. *SN Applied Sciences*, 2 (2): 276, 2020. doi: 10.1007/s42452-020-2070-3.
- [20] Roose T, Chapman SJ, Maini PK. Mathematical Models of Avascular Tumor Growth. *SIAM Review*, 49 (2): 179–208, 2007.
- [21] Wang Y, Lo W-C, Chou C-S. Modelling stem cell ageing: a multicompartiment continuum approach. *Royal Society Open Science*, 7: 191848, 2020.
- [22] Nakata Y, Getto P, Marciniak-Czochra A, Alarcón T. Stability analysis of multi-compartment models for cell production systems. *Journal of Biological Dynamics*, 6 (sup1): 2–18, 2012. doi: 10.1080/17513758.2011.558214.
- [23] Wu J, Fan Y, Tzanakakis ES. Increased Culture Density Is Linked to Decelerated Proliferation, Prolonged  $G_1$  Phase, and Enhanced Propensity for Differentiation of Self-Renewing Human Pluripotent Stem Cells. *Stem Cells and Development*, 24 (7): 892–903, 2015. doi: 10.1089/scd.2014.0384.
- [24] Alarcón T, Getto P, Marciniak-Czochra A, Vivanco M. A Model for Stem Cell Population Dynamics with Regulated Maturation Delay. *Discrete and Continuous Dynamical Systems, Supplement 2011*: 32–43, 2011.
- [25] Gaspari E, Franke A, Robles-Diaz D, Zweigerdt R, Roeder I, Zerjatke T, Kempf H. Paracrine mechanisms in early differentiation of human pluripotent stem cells: Insights from a mathematical model. *Stem Cell Research*, 32: 1–7, 2018.
- [26] Glauche I, Herberg M, Roeder I. Nanog Variability and Pluripotency Regulation of Embryonic Stem Cells - Insights from a Mathematical Model Analysis. *PLoS one*, 5 (6): e11238, 2010.
- [27] Stiehl T, Marciniak-Czochra A. Characterization of stem cells using mathematical models of multistage cell lineages. *Mathematical and Computer Modelling*, 53 (7-8): 1505–1517, 2011.

- [28] Marciniak-Czochra A, Stiehl T, Ho AD, Jäger W, Wagner W. Stem cells and development, 18 (3): 377–385, 2009.
- [29] Kirnasovsky OU, Kogan Y, Agur Z. Analysis of a Mathematical Model for the Molecular Mechanism of Fate Decision in Mammary Stem Cells. *Mathematical Modelling of Natural Phenomena*, 3 (7): 78–89, 2008.
- [30] Aguda BD, Friedman A. *Models of Cellular Regulation*. Oxford University Press, 2008. ISBN: 978-0-19-857091-2.
- [31] Pir P, Le Novère N. Mathematical Models of Pluripotent Stem Cells: At the Dawn of Predictive Regenerative Medicine. In: Schmitz U, Wolkenhauer O (eds) *Systems Medicine. Methods in Molecular Biology*, 1386. Humana Press, New York, NY, 2016. [https://doi.org/10.1007/978-1-4939-3283-2\\_15](https://doi.org/10.1007/978-1-4939-3283-2_15).
- [32] Wu PH, Giri A, Sun SX, Wirtz D. Three-dimensional cell migration does not follow a random walk. *Proceedings of the National Academy of Sciences USA*, 111 (11): 3949–3954, 2014. doi: 10.1073/pnas.1318967111.
- [33] Haderer KP. Reaction Transport Equations in Biological Modeling. *Mathematical and Computer Modelling*, 31 (4-5): 75–81, 2000.
- [34] Cai AQ, Landman KA, Hughes BD. Multi-scale modeling of a wound-healing cell migration assay. *Journal of Theoretical Biology*, 245 (3): 576–594, 2007.
- [35] Zaman MH, Kamm RD, Matsudaira P, Lauffenburger DA. Computational model for cell migration in three-dimensional matrices. *Biophysical Journal*, 89 (2): 1389–1397, 2005. doi: 10.1529/biophysj.105.060723.
- [36] Lemon G, Waters SL, Rose FRAJ, King JR. Mathematical modelling of human mesenchymal stem cell proliferation and differentiation inside artificial porous scaffolds. *Journal of Theoretical Biology*, 249 (3): 543–553, 2007.
- [37] Lemon G, King JR. Multiphase modelling of cell behaviour on artificial scaffolds: effects of nutrient depletion and spatially nonuniform porosity. *Mathematical Medicine and Biology: A Journal of the IMA*, 24 (1): 57–83, 2007.
- [38] Chung CA, Chen CP, Lin TH, Tseng CS. A compact computational model for cell construct development in perfusion culture. *Biotechnology and bioengineering*, 99(6): 1535–1541, 2008. doi: 10.1002/bit.21701.
- [39] Hillen T, Painter KJ. A user’s guide to PDE models for chemotaxis. *Journal of mathematical biology*, 58 (1-2): 183–217, 2009. doi: 10.1007/s00285-008-0201-3.

- [40] Keller EF, Segel LA. Model for chemotaxis. *Journal of Theoretical Biology*, 30 (2): 225–234, 1971.
- [41] Epshteyn Y, Xia Q. Efficient Numerical Algorithms Based on Difference Potentials for Chemotaxis Systems in 3D. *Journal of Scientific Computing*, 80, 26–59, 2019.
- [42] Kettemann A, Neuss-Radu M. Derivation and analysis of a system modeling the chemotactic movement of hematopoietic stem cells. *Journal of mathematical biology*, 56 (5): 579–610, 2008. doi: 10.1007/s00285-007-0132-4.
- [43] Keener J, Sneyd J. *Mathematical Physiology I: Cellular Physiology*. Springer-Verlag, New York, 2009.
- [44] Murray JD. *Mathematical Biology I. An Introduction*. Springer-Verlag, Berlin, 2002.
- [45] Murray JD. *Mathematical Biology II. Spatial Models and Biomedical Applications*. Springer-Verlag, Berlin, 2003.
- [46] Britton N. *Reaction-Diffusion Equations and their Applications to Biology*. Academic Press, London, 1986.
- [47] Britton N. *Essential Mathematical Biology*. Springer-Verlag, London, 2003.
- [48] Andreucci D, Bersani AM, Dell’Acqua G, Bersani E, De Lazzari C, Ledda M, Lisi A, Pontrelli G. A reaction-diffusion numerical model to predict cardiac tissue regeneration via stem cell therapy. *MASCOT11-IMACS/ISGG Workshop 2011*, IAC-CNR Rome Italy.
- [49] Marconi S, Ledda M, Bersani AM, Giorgio I, Lisi A, Bersani E, Andreucci D, Genuini I, Pisanelli DM, De Lazzari C. Multidisciplinary Approach to Myocardial Regeneration: In Vitro and In Silico Studies of Stem Cells Behaviour. *New Trends in Intelligent Software Methodologies, Tools and Techniques*. Fujita H and Herrera-Viedma E (eds), IOS Press, 2018.
- [50] Landman KA, Cai AQ. Cell Proliferation and Oxygen Diffusion in a Vascularising Scaffold. *Bulletin of Mathematical Biology*, 69: 2405–2428, 2007.
- [51] Shakeel M, Matthews PC, Graham RS, Waters SL. A continuum model of cell proliferation and nutrient transport in a perfusion bioreactor. *Mathematical Medicine and Biology*, 30 (1): 21–44, 2013. doi: 10.1093/imammb/dqr022.



- [52] McMurtrey R. Analytic Models of Oxygen and Nutrient Diffusion, Metabolism Dynamics, and Architecture Optimization in Three-Dimensional Tissue Constructs with Applications and Insights in Cerebral Organoids. *Tissue Engineering Part C*, 22 (3): 221–249, 2016.
- [53] Casciari JJ, Sotirchos SV, Sutherland RM. Glucose Diffusivity in Multicellular Tumor Spheroids. *Cancer Research*, 48: 3905–3909, 1988.
- [54] Casciari JJ, Sotirchos SV, Sutherland RM. Mathematical modelling of microenvironment and growth in EMT6/Ro multicellular tumour spheroids. *Cell Proliferation*, 25 (1): 1–22, 1992. doi: 10.1111/j.1365-2184.1992.tb01433.x.
- [55] Hwang NS, Varghese S, Elisseeff J. Controlled differentiation of stem cells. *Advanced Drug Delivery Reviews*, 60 (2): 199–214, 2008.
- [56] Guillot PV, Cui W, Fisk NM, Polak DJ. Stem cell differentiation and expansion for clinical applications of tissue engineering. *Journal of Cellular and Molecular Medicine*, 11 (5): 935–944, 2007.
- [57] Monod J. The growth of bacterial cultures. *Annual Review of Microbiology*, 3: 371–394, 1949. doi:10.1146/annurev.mi.03.100149.002103.
- [58] Mokhbi Soukane D, Shirazi-Adl A, Urban JPG. Computation of coupled diffusion of oxygen, glucose and lactic acid in an intervertebral disc. *Journal of Biomechanics*, 40 (12): 2645–2654, 2007.
- [59] Zhao F, Pathi P, Grayson W, Xing Q, Locke BR, Ma T. Effects of oxygen transport on 3-d human mesenchymal stem cell metabolic activity in perfusion and static cultures: experiments and mathematical model. *Biotechnol Prog*, 21(4): 1269–80, 2005.
- [60] Liu W, Hsin C, Tang F. A molecular mathematical model of glucose mobilization and uptake. *Mathematical Biosciences* 221 (2): 121–129, 2009.
- [61] Nyarko PR, Anokye M. Mathematical modeling and numerical simulation of a multiscale cancer invasion of host tissue. *AIMS Mathematics* 5 (4): 3111–3124, 2020.
- [62] Hill AV. The possible effects of the aggregation of the molecules of haemoglobin on its dissociation curves. *Journal of Physiology (London)* 40: Proceedings iv–vii, 1910.

- [63] Morgan PH, Preston Mercer L, Flodin NW. General model for nutritional responses of higher organisms. *Proc. Nat. Acad. Sci. USA*, 72 (11): 4327–4331, 1975.
- [64] COMSOL Multiphysics<sup>®</sup> Modeling Software: <https://uk.comsol.com/>
- [65] Amestoy PR, Duff IS, l'Excellent J-Y. Multifrontal parallel distributed symmetric and unsymmetric solvers. *Computer Methods in Applied Mechanics and Engineering*, 184 (2–4): 501–520, 2000.
- [66] Croll TI, Gentz S, Mueller K, Davidson M, O'Connor AJ, Stevens GW, Cooper-White JJ. Modelling oxygen diffusion and cell growth in a porous, vascularising scaffold for soft tissue engineering applications. *Chemical Engineering Science*, 60 (17), 4924–4934, 2005.
- [67] Brown DA, MacLellan WR, Laks H, Dunn JC, Wu BM, Beygui RE. Analysis of Oxygen Transport in a Diffusion-Limited Model of Engineered Heart Tissue. *Biotechnology and Bioengineering*, 97 (4): 962–975, 2007.
- [68] Wagner BA, Venkataraman S, Buettner GR. The rate of oxygen utilization by cells. *Free Radical Biology & Medicine*, 51, 700–712, 2011.
- [69] Shakeel M, Raza S. Nonlinear Computational Model of Biological Cell Proliferation and Nutrient Delivery in a Bioreactor. *Applied Mathematics* 5, 2284–2298, 2014.
- [70] Chung CA, Chen CW, Chen CP, Tseng CS. Enhancement of cell growth in tissue-engineering constructs under direct perfusion: Modeling and simulation. *Biotechnology and bioengineering*, 97 (6): 1603–1616, 2007. doi: 10.1002/bit.21378.
- [71] Rørth P. Collective cell migration. *Annual Review of Cell and Developmental Biology*, 25: 1, 407–429, 2009.
- [72] Rangarajan R, Zaman MH. Modeling cell migration in 3D. *Cell Adhesion & Migration*, 2 (2): 106–109, 2008.
- [73] Mogilner A. Mathematics of cell motility: have we got its number? *Journal of Mathematical Biology*, 58: 105–134, 2009.
- [74] Lo CM, Wang HB, Dembo M, Wang YL. Cell movement is guided by the rigidity of the substrate. *Biophysical Journal*, 79 (1): 144–152, 2000. doi:10.1016/S0006-3495(00)76279-5.

- [75] Ambrosi D, Bussolino F, Preziosi L. A review of vasculogenesis models. *Journal of Theoretical Medicine*, 6 (1): 1–19, 2005.
- [76] Sun S, Wheeler MF, Obeyesekere M, Patrick C. Multiscale Angiogenesis Modeling. In: Sunderam VS, van Albada GD, Sloot PMA, Dongarra J (eds) *Computational Science – ICCS 2005*. ICCS 2005. *Lecture Notes in Computer Science*, 3516. Springer, Berlin, Heidelberg. [https://doi.org/10.1007/11428862\\_13](https://doi.org/10.1007/11428862_13).
- [77] Fontelos MA, Friedman A, Hu B. Mathematical Analysis of a Model for the Initiation of Angiogenesis. *SIAM Journal on Mathematical Analysis* 33 (6): 1330–1355, 2002. doi: 10.1137/S0036141001385046.
- [78] Crapts LYD. Modelling an Angiogenesis Treatment After a Myocardial Infarction. M.Sc. Thesis. Delft University of Technology, The Netherlands. <http://resolver.tudelft.nl/uuid:bac4a3e4-f2ff-4ec2-aecb-333a579435f6>.
- [79] Milde F, Bergdorf M, Koumoutsakos P. A hybrid model for three-dimensional simulations of sprouting angiogenesis. *Biophysical journal*, 95 (7): 3146–3160, 2008. doi: 10.1529/biophysj.107.124511.
- [80] Chaplain MA, McDougall SR, Anderson AR. Mathematical modeling of tumor-induced angiogenesis. *Annual review of biomedical engineering*, 8: 233–257, 2006. doi:10.1146/annurev.bioeng.8.061505.095807.
- [81] MacArthur BD, Ma’ayan A, Lemischka IR. Systems biology of stem cell fate and cellular reprogramming. *Nature Reviews Molecular Cell Biology*, 10, 672–681, 2009.
- [82] Lei J, Levin SA, Nie Q. Mathematical model of adult stem cell regeneration with cross-talk between genetic and epigenetic regulation. *PNAS*, 111 (10) E880–E887, 2014.
- [83] Blum W, Henzi T, Schwaller B, Pecz L. Biological noise and positional effects influence cell stemness. *Journal of Biological Chemistry*, 293 (14), 5247–5258, 2018.
- [84] Pázdziorek PR. Mathematical Model of Stem Cell Differentiation and Tissue Regeneration with Stochastic Noise. *Bull. Math. Biol.*, 76, 1642–1669, 2014.
- [85] Ridden S. Stochastic models of stem cell dynamics. University of Southampton, Faculty of Social, Human and Mathematical Sciences, Doctoral Thesis, 157 pp., 2016.

- [86] Smith Q, Stukalin E, Kusuma S, Gerecht S, Sun SX. Stochasticity and Spatial Interaction Govern Stem Cell Differentiation Dynamics. *Scientific Reports*, 5, 12617, 2015.
- [87] Smith Q, Gerecht S. Extracellular Matrix Regulation of Stem Cell Fate. In *Stem Cell Switches and Regulators* (KK Hirschi, Section Editor). *Current Stem Cell Reports*, 4, 13–21, 2018.